Spontaneous formation of hierarchical wrinkles in Cr films deposited on silicone oil drops with constrained edges

Sen-Jiang Yu,[1,2,*] Yong-Ju Zhang,[3] Hong Zhou,[2] Miao-Gen Chen,[2] Xiao-Fei Zhang,[2] Zhi-Wei Jiao,[2] and Ping-Zhan Si[2]

[1]*Shanghai Key Laboratory of Special Artificial Microstructure Materials and Technology & Physics Department, Tongji University, Shanghai 200092, People's Republic of China*

[2]*Department of Physics, China Jiliang University, Hangzhou 310018, People's Republic of China*

[3]*Department of Physics, Taizhou University, Linhai 317000, People's Republic of China*

(Received 15 April 2013; revised manuscript received 6 September 2013; published 8 October 2013)

We report on the spontaneous formation of hierarchical wrinkling patterns in Cr films deposited on silicone oil drops with constrained edges. The appearance of the wrinkling patterns is strongly dependent on the film thickness and the size of the silicone oil drop. Because the Cr film at the drop edge is constrained due to the strong adhesion between the film and the glass surface, the wrinkle wavelength merely depends on the distance starting from the drop edge. When the distance increases, the wavelength increases quickly first, and then it slows down gradually in compliance with a simple power law. The evolution of the wrinkle amplitude is similar to that of the wavelength, but it is also closely related to the film thickness and the oil drop size. Based on the fact that the silicone oil is polymerized to form an elastic layer during deposition, the formation and evolution of the hierarchical wrinkling patterns have been analyzed in detail.

DOI: 10.1103/PhysRevE.88.042401 PACS number(s): 68.15.+e, 46.32.+x, 47.54.−r, 68.55.−a

I. INTRODUCTION

Buckling or wrinkling phenomena are very common in natural and artificial systems that span a wide range of scales, from macroscopic geologic structures [1], elastic sheets (or paper) [2], cloths (or curtains) [3], plant leafs (or flowers) [4], dried fruit [2], aging skin [5], biological tissue [4,6], to nanometer-scale structures such as various film-substrate bilayers and graphene [3,7]. The film-substrate bilayers are now widely used in many high-tech applications such as thermal barrier coatings, low-emissivity windows, and optical and microelectronic devices. In these bilayer structures, the buckling (or wrinkling) phenomena are found to result from the relief of internal stress and be strongly dependent on the nature of the substrate. For rigid substrates, buckle-driven delaminations such as straight-sided, circular, varicose, and telephone cord structures are usually observed [8–10]. For soft substrates, various wrinkling morphologies such as labyrinths, straight strips, herringbones, checkerboards, and hexagonal and triangular modes are frequently observed, where the film remains attached to the substrate [11–14]. When a solid film rests on a liquid substrate and is under a compressive stress, what will happen?

The vapor phase deposition of metals and organic molecules on a liquid substrate has been studied intensively in the past decade [15–20]. The results showed that the metal atoms, organic molecules, atomic clusters, and even a film piece can move freely on the liquid surface, which indicates that the interaction between the solid film and the liquid substrate in the tangent direction is very small [15,16]. A large variety of complex and ordered patterns caused by the internal stress are frequently observed in these nearly free-standing films, such as parallel sinusoidal cracks [17], band-shaped structures composed of a large number of rectangular domains [18,19], steplike creases [20], etc. These ordered stress patterns generally emerge in the films with millimeter dimensions and free edges.

Recent works also showed that when an elastic sheet floating on a liquid or soft (water for example) surface is compressed along two opposing edges, it may form sinusoidal wrinkles (under modest compression) or local folds (under further compression) [21–24], indicating that the confinement condition plays an important role in determining the stress patterns and mechanical responses of thin films [3,25]. In this paper, we report on the spontaneous formation of hierarchical wrinkling patterns in Cr films deposited on microscale silicone oil drops with constrained edges.

II. EXPERIMENT

The samples were prepared by a direct current (dc) magnetron sputtering technique at room temperature. Before deposition, some pure commercial silicone oil (Dow Corning 705 diffusion pump fluid with the vapor pressure below 10^{-8} Pa and the viscosity of about 175 mm^2/s at room temperature) was filled into a spraying apparatus. Then a large number of oil drops were sprayed onto a clean glass slide with an area of about 20×20 mm^2. The silicone oil can attach to the glass surface and form silicone oil drops with sizes spanning from several micrometers to more than a millimeter [see Fig. 1(a)]. The oil drops sprayed on the glass surface are a spherical cap in shape and the equilibrium contact angle is about 50° [26,27]. After deposition, the oil drops are somewhat flattened and the contact angle may decrease. Figure 1(b) shows the schematic view of a cross section of the silicone oil drop after the film deposition. Here the radius in plane is defined as the oil drop radius r and the distance starting from the drop edge is defined as x ($x \leqslant r$). It is clear that the thickness of the silicone oil in a drop is not uniform. The silicone oil is thickest in the central region and its thickness decreases to zero at the drop edge. The silicone oil drops can also be generated by dripping the silicone oil with a fixed volume onto the glass surface, which leads to similar experimental results.

*Corresponding author: sjyu@cjlu.edu.cn

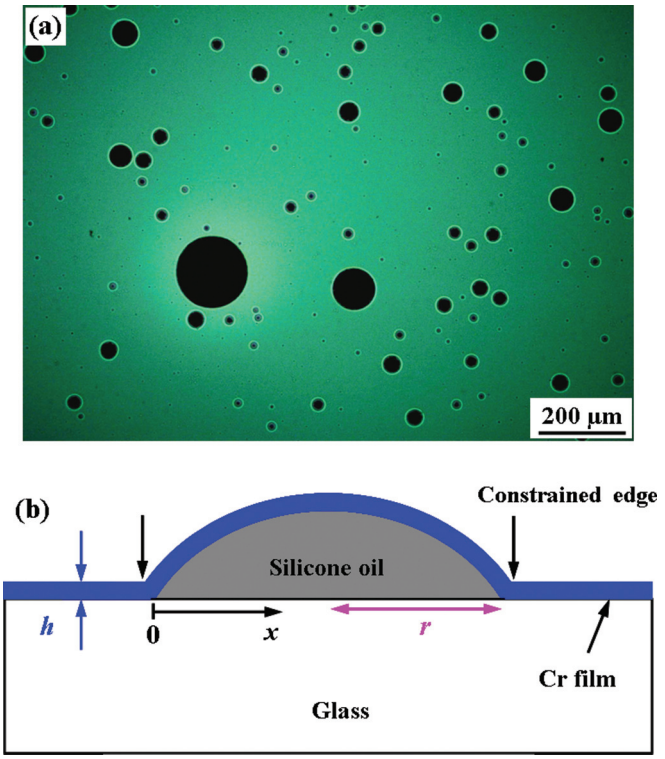

FIG. 1. (Color online) (a) Typical surface morphology of the film sample. The dark circles and bright region represent the Cr films deposited on silicone oil drops and the glass surface, respectively. (b) Schematic view of the cross section of the Cr film deposited on the silicone oil drop. The letters r, x, and h represent the oil drop radius in plane, the distance from the drop edge ($x \leqslant r$), and the thickness of the Cr film, respectively.

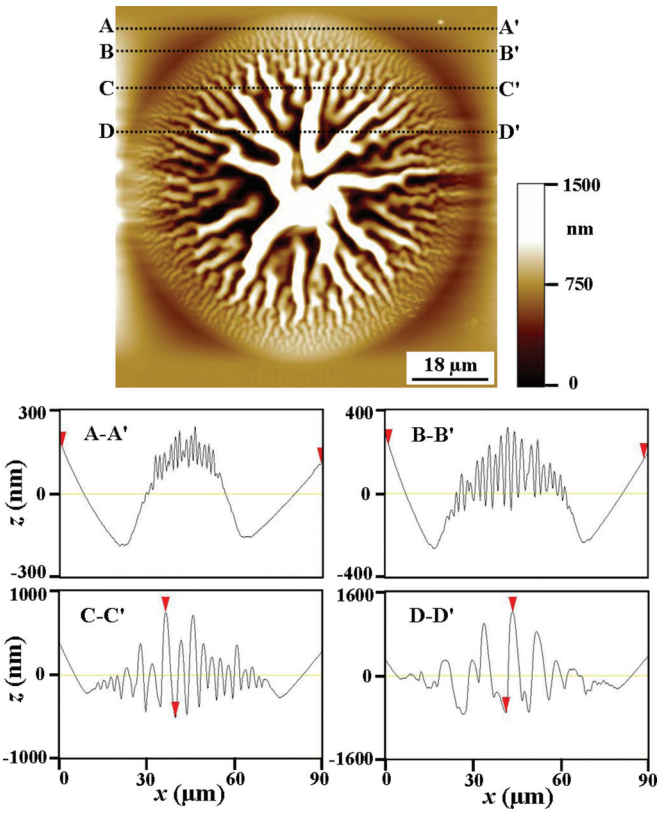

FIG. 2. (Color online) Typical AFM image (top) and corresponding profiles (bottom) of the Cr film on the silicone oil drop, $h = 100$ nm.

The sputtering target was a piece of chromium disk (purity 99.9%) with a diameter of 60 mm. The target-substrate distance was about 90 mm. The residual gas pressure before sputtering was below 4×10^{-4} Pa. The films were deposited under argon (purity 99.999%) in pressure of 0.5 Pa. The dc sputtering power was fixed to 120 W, corresponding to a deposition rate of $f \approx 20$ nm/min. The deposition time t ranged from 0.5 to 8 min, which was controlled precisely by a computer. After deposition, the film thickness h on the glass surface was calibrated by a profilometer (α-step 200 profilometer, Tencor). The surface morphologies of the samples were taken with an optical microscope (Leica DMLM) equipped with a charge-coupled device camera (Leica DC 300) which was interfaced to a computer for data storage and processing. The wrinkle morphologies and profiles were determined by an atomic force microscope (AFM, SPI3800N, Seiko) operated in tapping mode using an etched single-crystal Si tip with a radius of 10 nm. Collected data consisted of height information on square 256×256 arrays of pixels from area scans with lengths from 20 to 90 μm.

III. RESULTS AND DISCUSSION

A. Wrinkle morphology

The typical morphology of the sample is shown in Fig. 1(a), in which the dark circles and bright region represent the chromium (Cr) films deposited on silicone oil drops and the glass surface, respectively. In order to investigate more structural details of the film deposited on the oil drops, AFM images have been taken and the typical result is shown in Fig. 2. We find that the Cr film resting on the silicone oil drop is wrinkled, while the film deposited on the glass surface remains quite flat. The wrinkling patterns exhibit straight strips along the radial direction. When the distance x increases, the number density of the winkles obviously decreases. As a result, a characteristic hierarchical pattern appears.

Our experimental results show that the appearance of the wrinkling patterns strongly depends on the film thickness and the size of the oil drop. Figure 3 shows the evolution behavior of the wrinkling patterns with the film thickness when the size of the oil drop is fixed ($r \approx 35$ μm). It is clear that if the film thickness is quite small, the wrinkles only appear at the edge of the oil drop and they are always perpendicular to the edge. In the central region, however, the Cr film is comparatively smooth, as shown in Fig. 3(a). When the film thickness increases, the straight wrinkles propagate inwards and the number density of the straight wrinkles decreases gradually via coalescence, which results in the formation of the hierarchical pattern in the vicinity of the drop edge, as shown in Fig. 3(c). Furthermore, the Cr film in the central region is slightly wrinkled [see Figs. 3(b) and 3(c)]. When the film thickness is beyond a certain value, the wrinkles spread all over the oil drop, as shown in Fig. 3(d). When the film thickness increases further, the morphology of the wrinkling

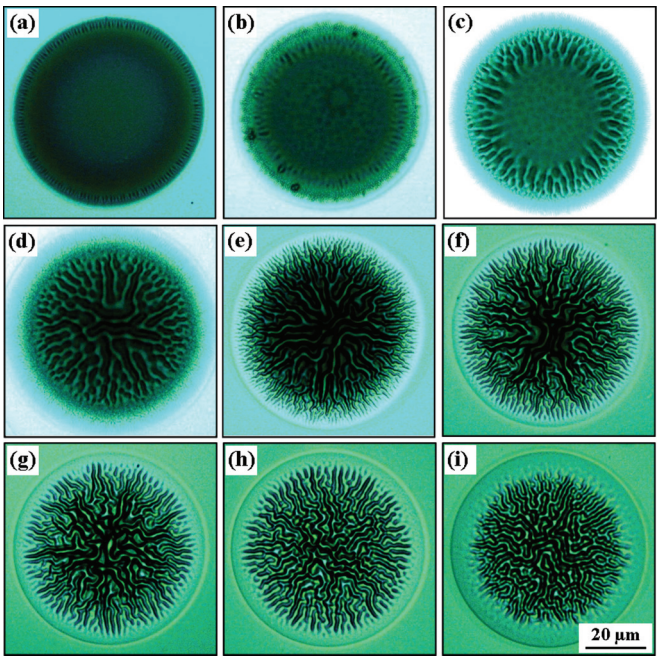

FIG. 3. (Color online) Evolution of the wrinkling patterns with the film thickness when the size of the oil drop is fixed ($r \approx 35\ \mu$m): (a) $h = 10$ nm; (b) $h = 20$ nm; (c) $h = 30$ nm; (d) $h = 40$ nm; (e) $h = 60$ nm; (f) $h = 80$ nm; (g) $h = 100$ nm; (h) $h = 120$ nm; (i) $h = 140$ nm. Each image has a size of $80 \times 80\ \mu$m^2.

patterns does not change greatly, but the Cr film in the vicinity of the drop edge becomes flattened and the unwrinkled region enlarges gradually, as shown in Figs. 3(f)–3(i).

Figure 4 shows the evolution behavior of the wrinkling patterns with the size of the oil drop when the film thickness is fixed (h=100 nm). We find that if the oil drop is quite small, no dominant wrinkle can be observed, as shown in Fig. 4(a). When the size of the oil drop is beyond a critical value (namely, the lower limit), the wrinkles start to appear in the center of the drop and they generally exhibit dimple shape, as shown in Fig. 4(b). When the size of the oil drop increases further, the wrinkles propagate outwards gradually, and finally, the hierarchical pattern composed of a larger number of straight wrinkles forms, as shown in Figs. 4(c)–4(f). Furthermore, it is clear that the unwrinkled region in the vicinity of the edge decreases gradually with increasing the size of the oil drop. Figure 5(a) shows the dependence of the width of the unwrinkled region w [see Fig. 4(b)] on the oil drop radius r. We find that when the radius r increases, the width w decreases drastically first, and then the decay speed slows down gradually and finally it approaches a stable value. The experimental data can be well fitted by the first-order exponential decay equation, i.e.,

$$w(r) = w(\infty) + w_{\text{decay}} e^{-r/r_0}, \tag{1}$$

where $w(\infty)$ represents the saturation width, w_{decay} represents the decreased value from $r = 0$ to infinitely large, and r_0 is a fitted constant, representing the decay rate of the width with the radius. In Fig. 5(a), $w(\infty)$, w_{decay} and r_0 are about 1.38, 10.41, and 19.86 μm, respectively. It should be noted here that Eq. (1) is valid only when the unwrinkled width w is smaller than the drop radius r. It can be seen from Fig. 3 that the unwrinkled region is also closely related to the film thickness. The quantitative relation between the unwrinkled width w and the film thickness h is shown in the inset of Fig. 5(a) when the size of the oil drop is fixed ($r \approx 35\ \mu$m). We find that the width w increases linearly with the film thickness when $h \geqslant 50$ nm. In the case of $h < 50$ nm, the unwrinkled width cannot be measured accurately in our experiment.

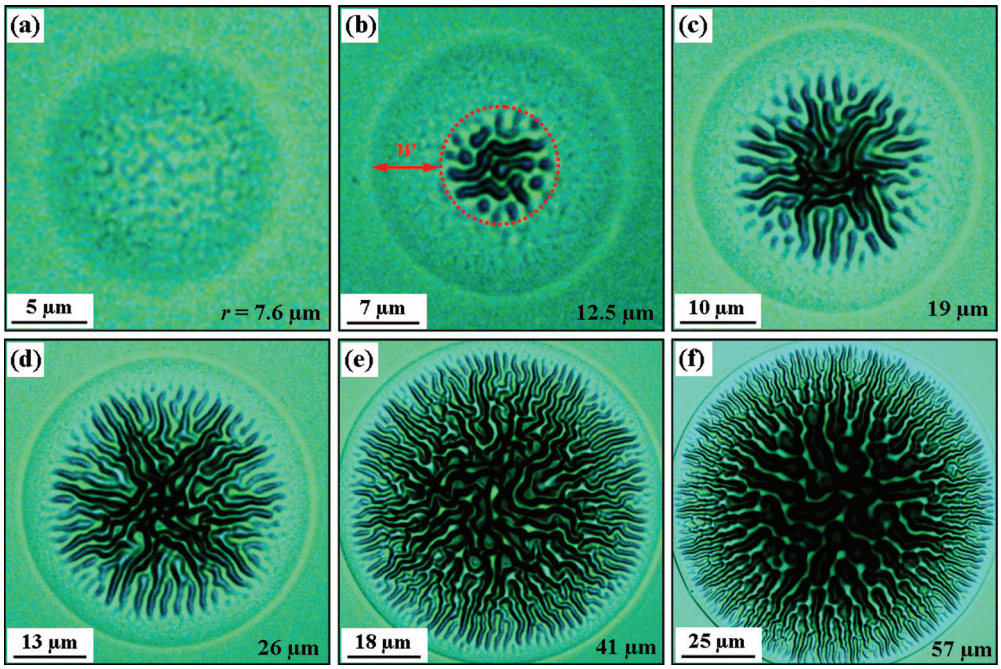

FIG. 4. (Color online) Evolution of the wrinkling patterns with the size of the oil drop when the film thickness is fixed ($h = 100$ nm). The value appearing in the bottom-right part of each image represents the radius of the oil drop. The letter w in (b) represents the width of unwrinkled ring near the drop edge.

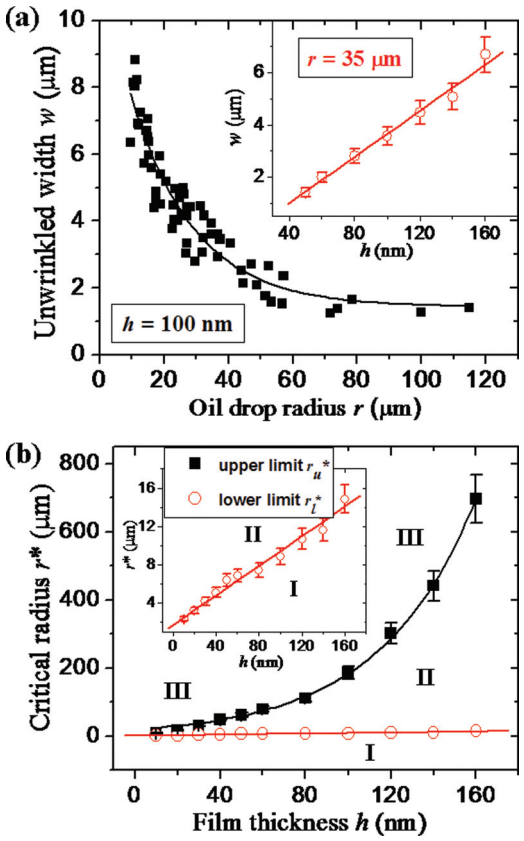

FIG. 5. (Color online) (a) Dependence of the width of the unwrinkled ring w on the oil drop radius r when the film thickness is fixed ($h = 100$ nm). The experimental data are fitted by the first-order exponential decay equation. The inset shows the dependence of the width w on the film thickness h when the size of the oil drop is fixed ($r \approx 35$ μm). The solid line is a linear fit to the experimental data. The error bars are standard deviations obtained from more than ten experimental data for each sample. (b) Dependence of the critical radius r^* (upper limit $r_u{}^*$ and lower limit $r_l{}^*$) on the film thickness h. The inset shows enlarged view of the lower limit curve. The red and black lines are linear and exponential ($r_u{}^* = r_{u0}e^{h/h_0}$) fits to the experimental data, respectively. The error bars are standard deviations obtained from more than ten experimental data for each sample.

Our experiment also shows that if the oil drop is too large to exceed an upper limit, the film in the center region does not wrinkle obviously, just as the cases shown in Figs. 3(a)–3(c). The critical values (upper limit $r_u{}^*$ and lower limit $r_l{}^*$) are strongly dependent on the film thickness. The quantitative relation between the critical radius r^* and the film thickness h is shown in Fig. 5(b). The upper limit $r_u{}^*$ increases quickly with the film thickness, and the experimental data can be well fitted by an exponential growth equation, i.e., $r_u{}^* = r_{u0}e^{h/h_0}$, where r_{u0} and h_0 are two fitted constants. On the contrary, the lower limit $r_l{}^*$ increases very slowly with the film thickness and the experimental data can be linearly fitted, as shown in the inset of Fig. 5(b). The upper limit and lower limit curves split the whole space into three parts: regions I–III. In the region below the lower limit (region I), which corresponds to larger film thickness and/or smaller oil drop, no dominant wrinkle appears, even in the center of the oil drop. In the region above the upper limit (region III), which corresponds to smaller film thickness and/or larger oil drop, no wrinkle can be observed or the wrinkles only appear in the vicinity of the edge. In the region above the lower limit and below the upper limit (region II), various hierarchical wrinkles form and they almost spread all over the oil drop, especially in the center region. When the film thickness increases, the upper limit increases quickly while the lower limit increases very slowly, and therefore the region II enlarges greatly, as shown in Fig. 5(b).

B. Formation mechanism

According to the previous studies [28,29], the temperature of the silicone oil would increase obviously during deposition owing to the heat radiation from the sputtering source and the bombardment of the depositing atoms. The temperature of the Cr film increases in a rate of 1 K/min, as detected by a thermocouple in contact with the back of the sample. The thermal stress of the Cr film can be expressed as [11]

$$\sigma = \frac{E_{\mathrm{f}}(\alpha_{\mathrm{s}} - \alpha_{\mathrm{f}})\Delta T}{1 - \nu_{\mathrm{f}}}. \tag{2}$$

Here the subscripts f and s refer to the film and the substrate, respectively, E is the elastic modulus, ν is the Poisson's ratio, α is the coefficient of thermal expansion, and ΔT is the temperature variation. For chromium, the elastic modulus and Poisson's ratio are about 250 GPa and 0.12, respectively. The coefficients of thermal expansion of the Cr film and the silicone oil substrate are about 6.2×10^{-6} and 7.9×10^{-4} K^{-1}, respectively. The varied temperature is in direct proportion to the deposition time. For the sample with $t = 8$ min ($h = 160$ nm), the temperature variation is about 8 K, and then the thermal stress of the Cr film can be estimated to be about 1.8 GPa. Therefore, the silicone oil substrate thermally expands during deposition owing to the temperature rise. After deposition, when the sample cools to room temperature, the silicone oil substrate thermally contracts and places the Cr film under a high compressive stress. Because the adhesion energy between the Cr film and the glass substrate is quite large in the film region outside of the oil drop, the drop edge can be regarded as a constrained edge condition [see Fig. 1(b)]. The constrained edge restricts outward spreading of the film and therefore the surface is wrinkled, as shown in Figs. 2–4.

Owing to the symmetry, the compressive stress in the center of the oil drop is uniform, which is relieved by formation of isotropic wrinkles. When an edge is present, the stress will no longer be uniform or equibiaxial. Bowden *et al*. have discussed the stress state near the film edge or relief step and the two stress components perpendicular and parallel to the film edge can be expressed as [11]

$$\sigma_x = -\sigma_0(1 - e^{-x/l}), \tag{3}$$

$$\sigma_y = -\sigma_0(1 - \nu_{\mathrm{f}}e^{-x/l}), \tag{4}$$

where σ_0 is the value of equibiaxial stress far away from the film edge (minus means that the stress is compressive), σ_x is the stress in the radial direction (perpendicular to the edge) and σ_y is the stress in the normal direction (along the circumference), and x is the distance starting from the drop edge. For chromium, the Poisson's ratio ν_{f} is about 0.12. It is clear that if $x = 0$, i.e., at the drop edge, $\sigma_x = 0$ and $\sigma_y = 0.88\sigma_0$. That is to say, only the normal stress component

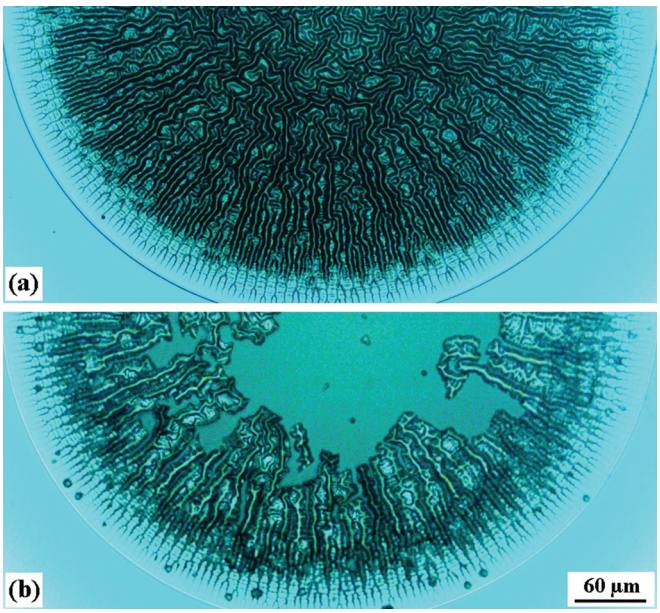

FIG. 6. (Color online) Comparison of the wrinkling morphologies before (a) and after (b) immersing of the sample into acetone for more than 10 minutes, $r = 275$ μm, $h = 100$ nm.

exists near the edge, which is relieved by formation of straight wrinkles perpendicular to the edge.

Many previous studies showed that the top surfaces of polymer substrates can be modified during deposition or exposure under ultraviolet, ozone, plasma, etc., perhaps by introducing new crosslinks by heat or cleaving of some organic bonds by deposition atoms and other high-energy particles [5,11,30,31]. We suggest that the top surface of the silicone oil is also polymerized to form an elastic (or somewhat "rigid") layer during deposition because the energy of the sputtering atoms is quite high (several electronvolts) and the temperature of the sample (especially the top surface of the oil drop) increases obviously. In order to confirm this suggestion, we have performed two simple tests in the experiment. First, the samples were immersed in acetone for more than ten minutes (the silicone oil can be easily dissolved into the acetone), and then washed by alcohol and taken under the optical microscope for morphology observation. It has been found that the wrinkling patterns in smaller drops are almost unchanged. For larger drops, the film in the center region is generally destroyed, while in the vicinity of the drop edge the wrinkling patterns remain unchanged, as shown in Fig. 6. Second, some drops were divided into two parts when the glass slide was cut with a glass cutter. If the section lines run across the smaller drops or in the vicinity of the edges of larger drops, the films and wrinkling patterns are almost unchanged. We obtained the cross sections of the wrinkling patterns by using optical microscopy and scanning electron microscopy (SEM), as shown in Fig. 7. When the section lines run across the central regions of larger drops, however, the films are always destroyed and no clear cross section can be obtained.

These two tests both indicate that the larger drop still contains much silicone oil, especially in the central region. During the immersion period, the silicone oil can be easily dissolved into the acetone and the film is destroyed. In the cutting test, the liquid phase (silicone oil) can flow freely and the film is also easily destroyed. For smaller drops or in the vicinity of the edge of larger drops, the structure and property of the silicone oil must have been modified and an elastic layer forms, which attaches well to the metal film and even attaches to the underlying glass surface. Therefore the elastic layer is no longer dissolved into the acetone during the immersion period and it can also keep stable during the cutting test. As a result, the films and the wrinkling patterns are almost unchanged in these cases.

Based on the experimental observations, we can conclude that during deposition, the modified elastic layer first forms on the top surface of the silicone oil drop, and then it spreads downward gradually. In addition, the rigidity (elastic modulus)

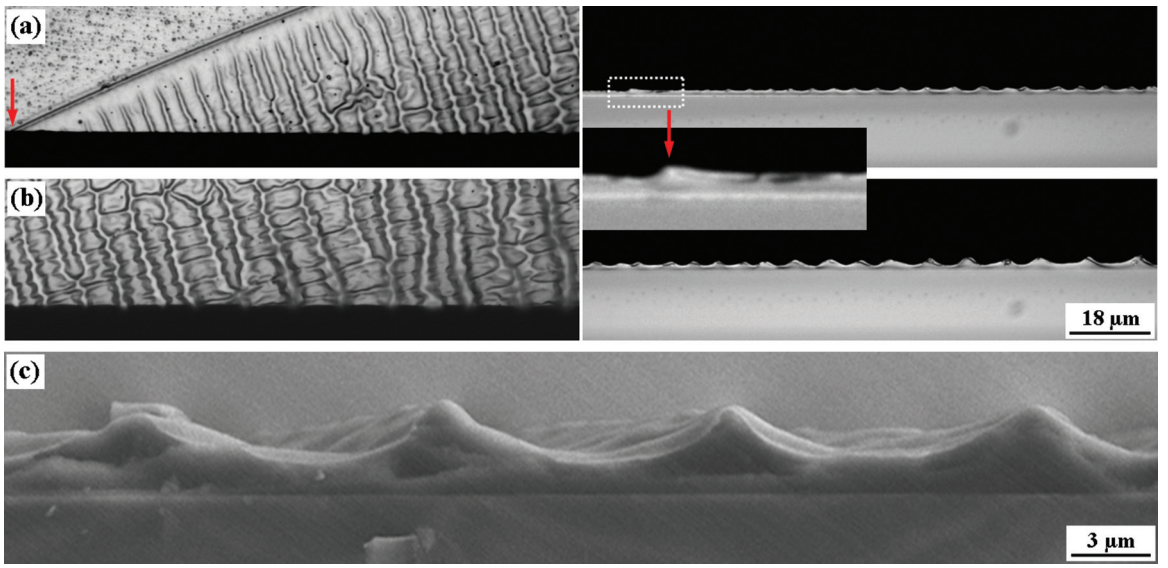

FIG. 7. (Color online) (a,b) Optical microscopic top views (left) and corresponding cross sections (right) of the wrinkling patterns appearing in a large oil drop when the section line runs in the vicinity of the drop edge. The inset shows enlarged view of the white box. The arrows represent the poison of the drop edge. (c) SEM cross section of the wrinkling patterns, $h = 160$ nm.

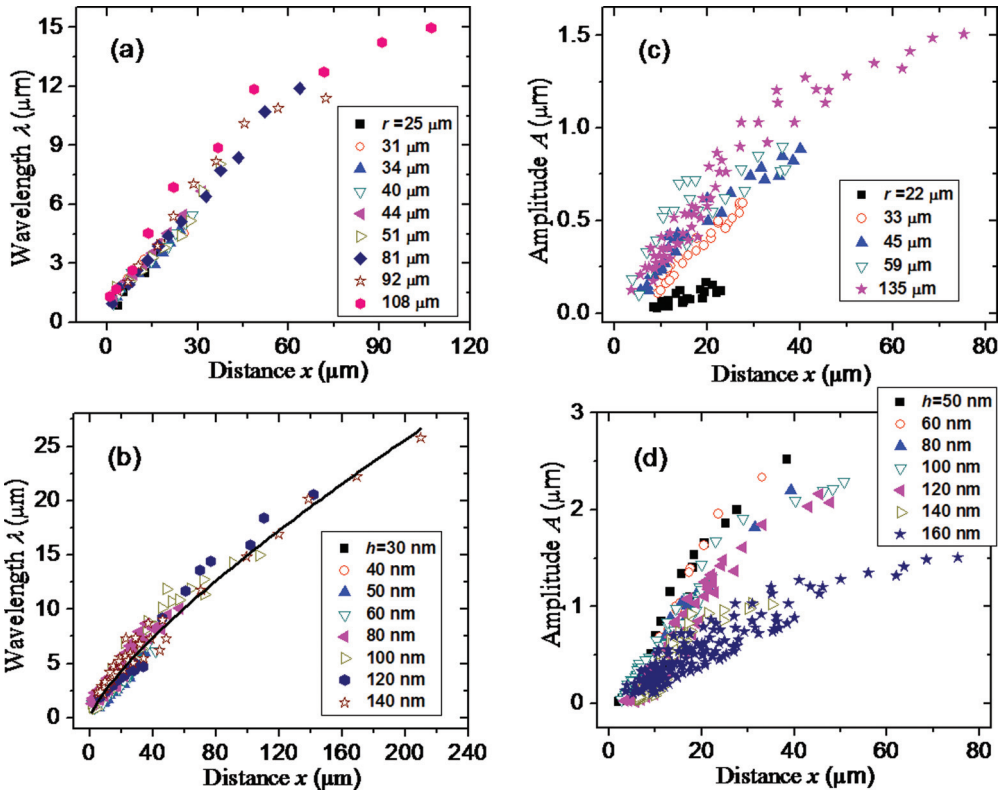

FIG. 8. (Color online) (a) Evolution of the average wavelength λ with the distance x for various radii when the film thickness is fixed ($h = 100$ nm). (b) Evolution of λ with x for different film thicknesses. The solid line is the fit to the experimental data with a scale power equation $\lambda = ax^b$. (c) Evolution of the average amplitude A with the distance x for various radii when the film thickness is fixed ($h = 160$ nm). (d) Evolution of A with x for different film thicknesses.

of the modified elastic layer decreases successively from top to bottom. Therefore, the average rigidity of the elastic layer should be closely related to the deposition time and the thickness of the silicone oil. It increases with increasing deposition time and decreases with increasing silicone oil thickness. Because the thickness of the silicone oil increases gradually with increasing the distance x, the average rigidity of the elastic layer should decrease successively from edge to center. Therefore the wrinkling patterns generally form at the edge first and then spread inwards gradually, as shown in Figs. 3(a)–3(d). During deposition, the elastic layer becomes more and more "rigid" so that the film cannot wrinkle obviously on this "rigid" substrate. Therefore the "rigid" region, which corresponds to the unwrinkled ring near the drop edge, increases with the film thickness when the size of the oil drop is fixed, as shown in Figs. 3(f)–3(i). The inset of Fig. 5(a) further indicates that the "rigid" region spreads inwards with an almost uniform speed during deposition.

Our experiment also shows that if the film thickness is large enough, the "rigid" region should spread all over the oil drop and no dominant wrinkle can be observed, especially in the center region, just as the case shown in Fig. 4(a). The critical radius (lower limit r_l^*) increases linearly with the film thickness [see the inset of Fig. 5(b)], proving that the "rigid" region spreads inwards uniformly during deposition once again. On the other hand, a larger oil drop generally possesses larger thickness. Therefore the "rigid" region decreases with increasing the size of the oil drop when the film thickness is fixed, as shown in Figs. 4 and 5(a). Finally, it should be emphasized that the thickness, structure, and property of the modified elastic layer cannot be determined accurately in the experiment, which makes it difficult to provide a more quantitative analysis.

C. Wrinkle wavelength and amplitude

The wavelength and amplitude of the wrinkles both increase obviously with increasing the distance from the drop edge (see the AFM profiles in Fig. 2). Figure 8 shows the quantitative dependences of the average wavelength λ and amplitude A on the distance x. For the same sample, the wrinkle wavelengths on the silicone oil drops with different radii almost coincide, especially in the vicinity of the drop edge [see Fig. 8(a)]. The wrinkle wavelengths for the samples with different film thicknesses are also located at the same curve [see Fig. 8(b)]. These results indicate that the wrinkle wavelength λ is almost independent of the oil drop size and the film thickness, but only depends on the distance x. When the distance x increases, the wavelength increases approximately linearly at the first stage, and then the speed slows down gradually. Furthermore, the experimental data can be well fitted by a scale power equation, i.e., $\lambda = ax^b$, where a and b are two fitted constants. In Fig. 8(b), a and b are about 0.43 μm and 0.77, respectively. On the other hand, the wrinkle amplitudes on the silicone oil drops with different radii for the same sample are somewhat

separated [see Fig. 8(c)]. Generally, when the radius increases, the amplitude A increases accordingly. Figure 8(d) shows that the amplitudes for the samples with different thicknesses are also separated greatly. Being similar to the evolution of the wavelength with the distance, the amplitude increases linearly with the distance x first, and then the speed slows down gradually.

Many previous works have utilized a spatially uniform, equibiaxial stress model to explain the wrinkling mechanism and estimate the mechanical properties [5,11–14,30,31]. The bilayer film system can be treated as a thin, stiff film on an infinite thick, homogeneous compliant substrate. The critical wavelength, that minimizes the total strain energy in the system, can be expressed by [5,11–14,30,31]

$$\lambda = 2\pi h\left[\frac{E_{\mathrm{f}}\left(1-\nu_{\mathrm{s}}^2\right)}{3E_{\mathrm{s}}\left(1-\nu_{\mathrm{f}}^2\right)}\right]^{1/3}. \tag{5}$$

Here h is the film thickness, E is the elastic modulus, and ν is the Poisson's ratio; the subscripts f and s refer to the film and substrate, respectively. It can be seen from Eq. (5) that the wavelength of the wrinkles depends only on the film thickness and the material properties of the film and substrate. When the elastic moduli and Poisson's ratios are fixed, the wavelength is directly proportional to the film thickness, which has been verified by many previous works [5,11–14,30,31]. Furthermore, Huang *et al*. have simulated the wrinkling morphologies in a disk under a uniform compressive stress [32]. They found that the radial strips form near the disk edge, which are similar to our experimental observations. However, the wrinkle wavelength is almost unchanged in the disk and no hierarchical pattern can be observed in their work.

It is clear that the above stress model cannot explain the wrinkle phenomenon existing in the Cr films resting on the silicone oil drops since the wavelength is independent of the film thickness [see Fig. 8(b)]. The discrepancy may be due to two possible reasons: the finite thick substrate or the constrained edge. Recently Yoo *et al*. studied the influence of the substrate thickness on the wrinkle wavelength when the substrate thickness is finite and of the same order of magnitude as the film [33,34]. They found that the wrinkle wavelength is not only related to the film thickness, but also dependent on the substrate thickness in this case. When the film thickness is fixed, the wavelength increases with increasing the substrate thickness, the same as the evolution behavior of the wavelength in our experiment. However, the SEM image shows that the thickness of the silicone oil layer (more precisely, the modified elastic layer) is of the order of 1 μm, at least 1–2 orders in magnitude larger than that of the film [see Fig. 7(c)]. Since the thickness of the substrate is much larger than that of the film, the substrate thickness should not be responsible for the evolution behavior of the wavelength. Furthermore, if the substrate thickness is a dominant effect, the wavelength should be separated greatly for the oil drops with different radii since the oil thicknesses are quite different.

Therefore, we can draw a conclusion that the finite substrate thickness should not be dominant in our experiment, and on the contrary, the second reason (constrained edge effect) may be responsible for the hierarchical wrinkling pattern. We suggest that the Cr film tends to adopt a larger wavelength while the constrained edge limits the development of the wavelength. It is clear that when the distance from the drop edge increases, the constraint effect becomes weak and the wavelength increases gradually, which results in the formation of the hierarchical wrinkling pattern. Similar hierarchical patterns have been observed in constrained thin sheets such as suspended graphene, curtains, and bilayers [3,4,12,25]. Furthermore, many previous theoretical studies showed that the hierarchical pattern exhibits a self-similarity and can be described by a simple power law [3,35], which can also be observed in our experiment [see Fig. 8(b)].

On the other hand, previous works have shown that the wrinkle amplitude A is not only dependent on the wrinkle wavelength λ, but also related to the strain of the substrate ε, which can be expressed as $A \propto \lambda\sqrt{\varepsilon}$ [2,5]. Because the amplitude is mainly determined by the wavelength, the evolution behavior of the amplitude with the distance is similar to that of the wavelength. But the amplitude is also proportional to the square root of ε and thus it is separated greatly for different oil drop radii and different film thicknesses, as shown in Figs. 8(c) and 8(d). The relation between the strain ε and the compressive stress σ of the Cr film can be expressed as $\sigma = \varepsilon\bar{E}$, where $\bar{E}$ is the equivalent elastic modulus of the substrate. As we have mentioned above, if the film thickness is fixed, the thermal stress σ is equal for different oil drops. When the size of the oil drop increases, the equivalent elastic modulus $\bar{E}$ decreases and thus the strain ε increases. Therefore the amplitude increases with the radius of the oil drop, as shown in Fig. 8(c). Because the dominant wrinkles almost disappear for the smaller oil drops (for example, $r = 22$ μm), the separation of the amplitudes between $r = 22$ and 33 μm is quite large. Our experiment also shows that when the oil drop is beyond a certain value, the amplitudes for different radii almost coincide [see Fig. 8(c)], indicating that the equivalent elastic modulus $\bar{E}$ (or the strain ε) changes slightly for larger silicone oil drops. Because the equivalent elastic modulus $\bar{E}$ increases gradually during deposition, it is reasonable that the amplitude A decreases with increasing the film thickness, as shown in Fig. 8(d).

IV. CONCLUSIONS

In summary, ordered hierarchical wrinkling patterns, spontaneously forming in Cr films deposited on silicone oil drops with constrained edges, are described and discussed in detail. The wrinkles always exhibit straight strips perpendicular to the perimeter. The wrinkle morphologies are closely related to the film thickness and the size of the oil drop. The formation of the wrinkling patterns results from the thermal contraction of the oil drop after deposition. The wrinkle wavelength is almost independent of the film thickness and the oil drop size, but only depends on the distance starting from the drop edge. The evolution of the wavelength with the distance can be described by a simple power law and can be attributed to the constrained edge effect. On the other hand, the wrinkle amplitude not only depends on the distance, but also relates to the film thickness and the oil drop size. The amplitude evolutions as well as the wrinkling morphologies can be well explained based on the fact that

the silicone oil is polymerized to form an elastic layer during deposition. We anticipate that the metal films deposited on microscale silicone oil drops will provide a test bed not only for fundamental research on the influence of the constrained edge on the wrinkling patterns, but also for technological applications in optical devices and microelectromechanical systems (MEMS), etc.

ACKNOWLEDGMENTS

We thank Chun-Qiang Chen and Quan-Lin Ye for useful discussions and technical assistance. This work was supported by the National Natural Science Foundation of China (Grants No. 11204283, No. 11074227, and No. 51271172) and Zhejiang Provincial Natural Science Foundation (Grants No. R6110362 and No. LQ13A040002).

[1] F. S. Jeng, M. L. Lin, Y. C. Lai, and M. H. Teng, J. Struct. Geol. **24**, 501 (2002).
[2] E. Cerda and L. Mahadevan, Phys. Rev. Lett. **90**, 074302 (2003).
[3] H. Vandeparre, M. Piñeirua, F. Brau, B. Roman, J. Bico, C. Gay, W. Bao, C. N. Lau, P. M. Reis, and P. Damman, Phys. Rev. Lett. **106**, 224301 (2011).
[4] B. Li, Y.-P. Cao, X.-Q. Feng, and H. Gao, Soft Matter **8**, 5728 (2012).
[5] J. Genzer and J. Groenewold, Soft Matter **2**, 310 (2006).
[6] E. Hannezo, J. Prost, and J.-F. Joanny, Phys. Rev. Lett. **107**, 078104 (2011).
[7] W. Bao, F. Miao, Z. Chen, H. Zhang, W. Jang, C. Dames, and C. N. Lau, Nat. Nanotechnol. **4**, 562 (2009).
[8] F. Foucher, C. Coupeau, J. Colin, A. Cimetière, and J. Grilhé, Phys. Rev. Lett. **97**, 096101 (2006).
[9] J. Colin, C. Coupeau, and J. Grilhé, Phys. Rev. Lett. **99**, 046101 (2007).
[10] J.-Y. Faou, G. Parry, S. Grachev, and E. Barthel, Phys. Rev. Lett. **108**, 116102 (2012).
[11] N. Bowden, S. Brittain, A. G. Evans, J. W. Hutchinson, and G. M. Whitesides, Nature (London) **393**, 146 (1998).
[12] H. Vandeparre and P. Damman, Phys. Rev. Lett. **101**, 124301 (2008).
[13] Y. Ni, L. He, and Q. Liu, Phys. Rev. E **84**, 051604 (2011).
[14] B. Audoly and A. Boudaoud, J. Mech. Phys. Solids **56**, 2422 (2008).
[15] G.-X. Ye, Th. Michely, V. Weidenhof, I. Friedrich, and M. Wuttig, Phys. Rev. Lett. **81**, 622 (1998).
[16] M. Voigt, S. Dorsfeld, A. Volz, and M. Sokolowski, Phys. Rev. Lett. **91**, 026103 (2003).
[17] P.-G. Cai, S.-J Yu, X.-J. Xu, M.-G. Chen, C.-H. Sui, and G.-X. Ye, Appl. Surf. Sci. **255**, 8352 (2009).
[18] Q.-L. Ye, X.-J. Xu, P.-G. Cai, A.-G. Xia, and G.-X. Ye, Phys. Lett. A **318**, 457 (2003).
[19] S.-J. Yu, Y.-J. Zhang, Q.-L. Ye, P.-G. Cai, X.-W. Tang, and G.-X. Ye, Phys. Rev. B **68**, 193403 (2003).
[20] X. Liu and M. Wuttig, Phys. Rev. B **73**, 033405 (2006).
[21] L. Pocivavsek, R. Dellsy, A. Kern, S. Johnson, B. Lin, K. Y. C. Lee, and E. Cerda, Science **320**, 912 (2008).
[22] B. D. Leahy, L. Pocivavsek, M. Meron, K. L. Lam, D. Salas, P. J. Viccaro, KaYee C. Lee, and B. Lin, Phys. Rev. Lett. **105**, 058301 (2010).
[23] T. J. W. Wagner and D. Vella, Phys. Rev. Lett. **107**, 044301 (2011).
[24] J. Zang, X. Zhao, Y. Cao, and J. W. Hutchinson, J. Mech. Phys. Solids **60**, 1265 (2012).
[25] H. Vandeparre, S. Desbief, R. Lazzaroni, C. Gay, and P. Damman, Soft Matter **7**, 6878 (2011).
[26] S. R. Ranabothu, C. Karnezis, and L. L. Dai, J. Colloid Interface Sci. **288**, 213 (2005).
[27] A. Al-Shareef, P. Neogi, and B. Bai, Chem. Eng. Sci. **99**, 113 (2013).
[28] X.-M. Tao, G.-X. Ye, Q.-L. Ye, J.-S. Jin, Y.-F. Lao, and Z.-K. Jiao, Phys. Rev. B **66**, 115406 (2002).
[29] S.-J. Yu, H. Zhou, Y.-J. Zhang, M.-G. Chen, Z.-W. Jiao, and P.-Z. Si, Thin Solid Films **520**, 5683 (2012).
[30] C. M. Stafford, C. Harrison, K. L. Beers, A. Karim, E. J. Amis, M. R. VanLandingham, H. C. Kim, W. Volksen, R. D. Miller, and E. E. Simonyi, Nat. Mater. **3**, 545 (2004).
[31] K. Efimenko, M. Rackaitis, E. Manias, A. Vaziri, L. Mahadevan, and J. Genzer, Nat. Mater. **4**, 293 (2005).
[32] Z. Y. Huang, W. Hong, and Z. Suo, J. Mech. Phys. Solids **53**, 2101 (2005).
[33] P. J. Yoo, K. Y. Suh, S. Y. Park, and H. H. Lee, Adv. Mater. **14**, 1383 (2002).
[34] P. J. Yoo, Electron. Mater. Lett. **7**, 17 (2011).
[35] S. Conti, A. DeSimone, and S. Müller, Comput. Methods Appl. Mech. Eng. **194**, 2534 (2005).